



Evaluation of sintered bauxite proppant for binary enhanced geothermal systems

Bijay KC · Ehsan Ghazanfari · John McLennan ·
Luke P. Frash · Meng Meng

Received: 23 September 2023 / Accepted: 11 December 2023
© The Author(s) 2024

Abstract Solid granular proppant particles are widely used in oil and gas development to sustain permeability through fractures after hydraulic stimulation. Similar proppants are of interest for geothermal applications where the goal of sustaining permeability is the same, but the harsh geothermal environment risks rapid proppant degradation that will reduce fracture permeability. Here, we present proppant conductivity experiments using saw cut granite, tensile fractured granite, and aluminum control specimens packed with sintered bauxite ceramic proppants at concentrations of 0.0, 0.1, and 1.0 kg/m². Simulated geothermal conditions included temperatures up to 130 °C and normal closure stresses up to 60 MPa. Compared to unpropped specimens, peak fracture conductivity enhancement was up to 6 orders of magnitude. At simulated geothermal conditions, proppants were able to sustain fracture conductivity

over 60 h, but chemical dissolution and decreasing permeability over time were evident. Irreversible conductivity reductions with crushing and embedment of proppants during loading stages were also observed. Overall, sintered bauxite proppant remains a promising option for low-temperature binary-cycle enhanced geothermal systems.

Article highlights

1. Sintered bauxite proppant holds promise to enhance and sustain fracture conductivity under low-temperature EGS conditions.
2. Proppant crushing and embedment lead to irreversible conductivity decline.
3. Mineral dissolution from proppant and rock fracture will diminish the benefit of proppant over time.

B. KC (✉) · L. P. Frash · M. Meng
Los Alamos National Laboratory, Los Alamos, NM 87545,
USA
e-mail: bkc@lanl.gov

B. KC · E. Ghazanfari
Department of Civil and Environmental Engineering,
University of Vermont, 33 Colchester Ave., Burlington,
VT 05405, USA

J. McLennan
Department of Chemical Engineering, University of Utah,
423 Wakara Way, Suite 300, Salt Lake City, UT 84108,
USA

Keywords Proppant pack conductivity · Hydraulic fracturing · Stress cycle · Dissolution

1 Introduction

Geothermal energy is a clean and reliable source of energy that has emerged as a viable source for base-load electricity. In 2021, geothermal power plants in the United States produced about 16 TWh, which is 0.4% of the utility scale electricity generation in the

country (EIA 2022). Most of the current geothermal plants generating electricity use conventional hydrothermal systems, which contain hot fluid (or vapor) and adequate permeability for economic production of electricity. Such systems are only feasible in certain geological regions and only represents a small portion of the total geothermal resources around the world (Xu et al. 2004; Bradford et al. 2013; Rutqvist et al. 2016). In contrast, the vast majority of the remaining geothermal resources have sufficient heat but lack the required permeability to be economically produced using conventional methods. These resources require stimulation to create engineered fracture networks for economic extraction of energy (Tester et al. 2006; Williams et al. 2008; Ghassemi 2012). Stimulated geothermal reservoirs are known as Enhanced Geothermal Systems (EGS; Häring et al. 2008; Cladouhos et al. 2016; Schill et al. 2017; Tomac and Sauter 2018). If these EGS reservoirs can be successfully tapped, Augustine et al. (2019) estimates that the USA will have 60 GW_e of installed geothermal capacity by the year 2050.

When new fractures are created or existing fractures are stimulated for EGS, the increased permeability of these fractures must be sustained over time to enable heat extraction. Promising methods to sustain this increased fracture permeability include injecting proppant particles, shear asperity propping, high-pressure propping, and acid treatments (Portier et al. 2009; Cladouhos et al. 2016; Ye and Ghassemi 2018; Bijay and Ghazanfari 2021; Frash et al. 2023a). Injecting solid proppant particles such as sand or bauxite grains is hoped to sustain fracture permeability in the long-term even after the release of injection pressure (Liang et al. 2016). Moreover, proppant eliminates the necessity of fracture sliding (i.e., shearing) during hydraulic stimulation which would rely on having the Goldilocks mix of multiple suitably weak, suitably oriented, sufficiently permeable (but not too permeable), appropriately positioned pre-existing fractures and adequate in-situ shear stress to mobilize these fractures without inadvertently inducing an earthquake (Meng et al. 2022). However, proppant is not without its own limitations.

Effective permeability of proppant packs depend on good placement of particles within the fracture network and the particles and are known to have challenges with decreasing permeability over time due to crushing, fines migration, embedment, and chemical

degradation (Bandara et al. 2019; Barboza et al. 2021). A wide range of proppant particle types have been developed to combat these problems, including natural sand, ceramics, resin-coatings, and bauxite (Liang et al. 2016). These advancements helped proppant to achieve success in unconventional oil and gas stimulations to sustain the conductivity of stimulated fractures (Wang et al. 2018; Bandara et al. 2020) but the applicability of proppant in harsh high-temperature hard-rock high-stress EGS is unclear and unproven (Penny 1987; Bandara et al. 2019). In addition, proppant in EGS reservoir must maintain higher permeability than for oil and gas applications and it must maintain it for longer durations to be economic (Frash et al. 2023b). However, experience with proppant use in geothermal fields is limited (Huenges et al. 2004; Zimmermann and Reinicke 2010) so its long-term performance to sustain the fracture in geothermal reservoir remains unknown.

Proppant performance in EGS has been investigated through numerical modeling, laboratory tests, and limited field scale testing (Huenges et al. 2004; Shiozawa et al. 2014; Zhang et al. 2022). Laboratory scale tests are used as a proxy to simulate proppant performance under in-situ EGS conditions. To evaluate chemical stability, prior laboratory experiments immersed mixtures of proppant and crushed granite in fluid at elevated temperature for extended time to measure mineral precipitation/dissolution and proppant degradation (McLin et al. 2010; Brinton et al. 2011; Jones et al. 2014). To evaluate mechanical strength against crushing and embedment, laboratory experiments have been conducted on proppant packs (Fredd et al. 2000; Bandara et al. 2021; Zhang et al. 2022). This work showed that crushing and embedment depends upon the in-situ conditions, such as the total stress applied to the fracture, effective stress in the proppant pack, fluid composition, and temperature. Proppant selection (e.g. sand versus bauxite) and proppant concentration (i.e., proppant loading or layer thickness) are also primary parameters that control long-term permeability (Bandara et al. 2019). High strength ceramic proppant such as sintered bauxite are promising for field applications because this material is more mechanically and chemically stable than other proppants such as quartz sand at elevated temperature (Liang et al. 2016; Bandara et al. 2019). Higher concentrations of proppant minimize crushing and embedment (Tang et al. 2018) but such high

concentrations are difficult to achieve far away from the injection point (Sahai and Moghanloo 2019; Chun et al. 2020).

In this study, we evaluate the performance of low concentration sintered bauxite proppant at EGS reservoir conditions to assess the suitability of this material for field application. We conducted a suite of experiments on saw cut granite, rough fractured granite, and aluminum control specimens. Each specimen included a central diametric fracture packed with proppant at three different concentrations. Proppant pack conductivity was measured at an elevated temperature of 130 °C over 60 h during which time the specimen was subjected to an incremental stress cycle. Post test investigation included scanning electron microscopy (SEM) to evaluate embedment and crushing along with effluent aqueous chemistry to monitor dissolution. Our results will show that sintered bauxite does sustain permeability over 60 h, but this material does degrade significantly over this time. Proppant performance will be shown to improve with thicker proppant packs and in rougher surfaced fractures.

2 Materials and methods

2.1 Rock specimens

Quarried hard crystalline granite sourced from Barre, Vermont, was selected for our experiments because granite is the most common basement rock type that is anticipated for EGS resources (Häring et al. 2008; Tomac and Sauter 2018). Moreover, our samples were fresh and unweathered to better mimic deep in-situ conditions (Bijay and Ghazanfari 2021). X-Ray Diffraction (XRD) analysis of the Barre granite indicated that this granite is composed of 42.4% quartz, 36.7% oligoclase, 11.2% microcline, 3.9% biotite, 3.2% muscovite, and 2.6% accessory minerals including oxides, calcite, and chlorite (Caulk et al. 2016). This Barre granite had a dry density of $2.63 \text{ g/cm}^3 \pm 0.1 \text{ g/cm}^3$, and porosity of $0.72\% \pm 0.15\%$. Both saw-cut and fractured granite specimens were prepared. As an experiment control, a saw cut aluminum specimen was also prepared.

To prepare 38.1 mm diameter cylindrical specimens for the experiments, blocks of Barre granite were split by a tensile fracture (i.e., rough fracture) or

with a saw cut (i.e., smooth fracture) along the center of the block (Fig. 1). A chisel in a hydraulic press was used to tensile fracture the block. Cylindrical specimens were cored from the fractured blocks such that the specimen would contain a single horizontal fracture at its center. The two ends of the specimen were polished to 0.025 mm surface flatness and parallelity. Two 3.2 mm diameter bore holes were drilled, one in each opposing half of the specimen, to serve as a flow path from the end face to the fracture surface. The aluminum specimen was simpler being a machine cut of a round aluminum stock on the center. The final total of three specimens are shown in Fig. 2 with details summarized in Table 1.

2.2 Proppants

Sintered bauxite 40/70 mesh (nominal particle sizes from 210 to 400 μm) proppant was selected for our study because of its high strength and low chemical reactivity (Liang et al. 2016; Bandara et al. 2020). The proppant size should be smaller than the fracture aperture in the field so that the proppant can enter the fracture during stimulation. Our selected proppant size is comparable to what was successfully injected at the Blue Mountain Geothermal field, where mixture of 100 and 40/70 mesh silica sand was used (Norbeck et al. 2023). Moreover, sintered bauxite proppant is expected to be stable at elevated temperatures (Bagepalli et al. 2020) making it promising for EGS application. This proppant's bulk density was 2.1 g/cm^3 with a specific gravity of 3.6. The published American Petroleum Institute (API) crush value for this proppant at 100 MPa (15,000 psi) was 2.8. Due to its high crush strength, this proppant is expected to withstand the high stresses of EGS reservoir without crushing when compared to commonly used proppant such as Ottawa sand which has crush value of 13.3 at 9000 psi (62 MPa) (e.g., Benson and Wilson 2015). As shown in Fig. 2, the proppant particles are spherical in shape which makes them more ideal to resisting crushing.

2.3 Specimen assembly

The selection of a proppant concentration and the method to distribute proppant within a fracture is a known challenge for both the laboratory and the field. For example, the distribution of proppant mass in a

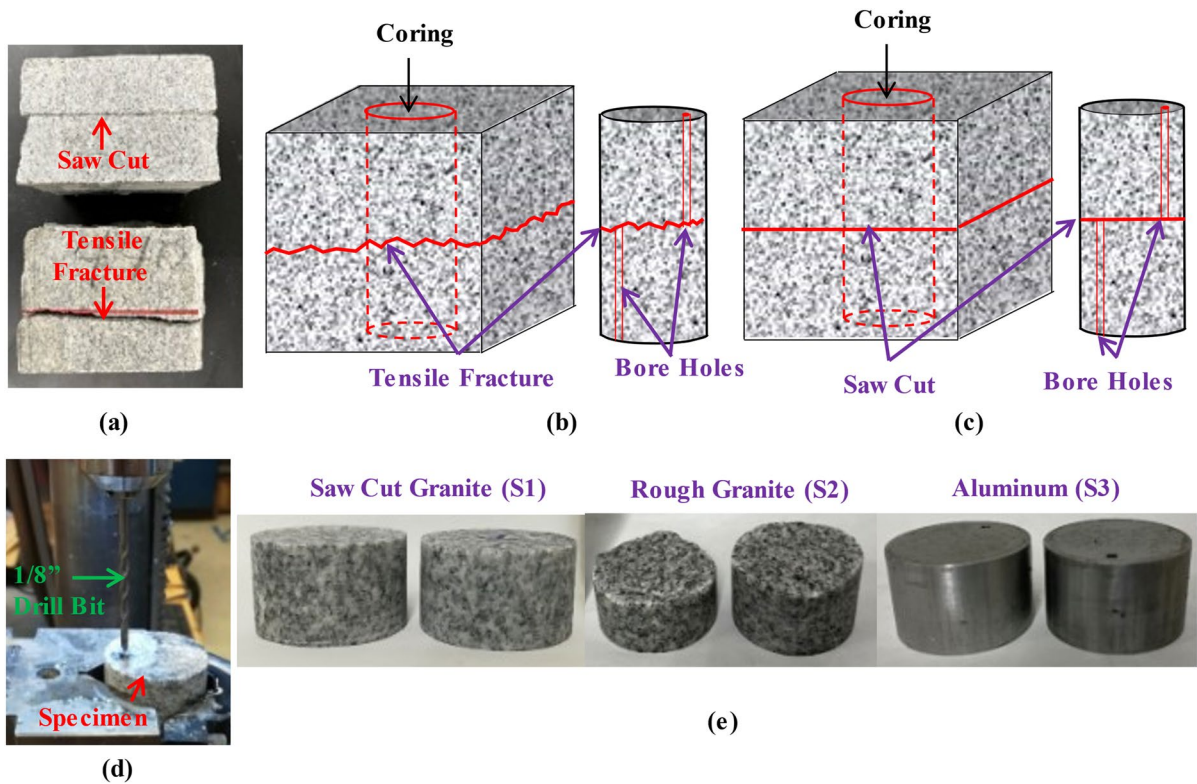


Fig. 1 Cylindrical specimens were prepared from **a** granite blocks with fractures or saw cuts that were **b**, **c** cored to include fractures across the diameter at each specimen's center.

Next, **d** holes for fluid paths were drilled. This produced **e** the final three specimens ready for experiments

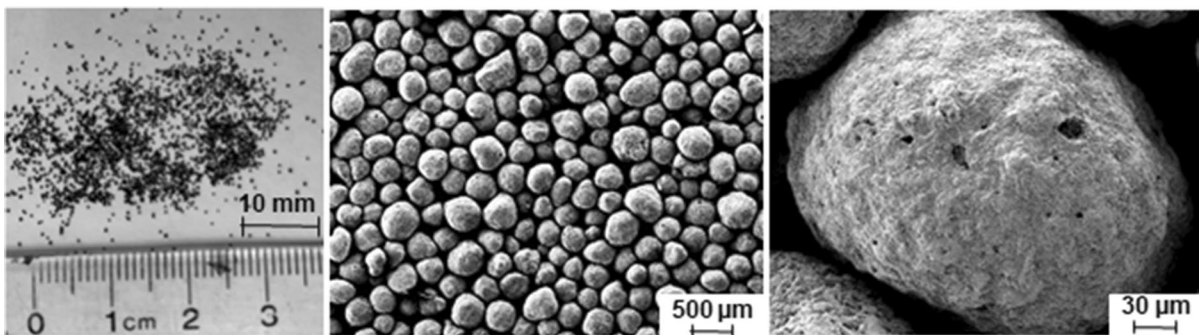


Fig. 2 Sintered bauxite 40/70 proppant enlarged to show texture and sphericity

fracture, or set of fractures, will vary as a function of numerous parameters (e.g., proppant injection schedule), some of which are uncontrollable (e.g., surface roughness). To simplify this challenge, we placed proppant in the fracture with different concentrations as a function of area. More specifically, we targeted

proppants loading of 1.0, 0.1, and 0.0 kg/m² because this has been suggested as adequate in previous literature (Fredd et al. 2000). This allows for a more direct comparison of our laboratory data to field values that can be estimated using models. However, this does not imply uniform proppant distribution within

Table 1 Specimen details

ID	Material	Fracture surface	Diameter (mm)	Length (mm)	Proppant pack thickness (mm)	
					0.1 kg/m ²	1 kg/m ²
S1	Granite	Saw cut	38.1	42.67	0.18	0.28
S2	Granite	Rough	38.1	41.23	0.29	0.40
S3	Aluminum	Smooth	38.1	40.00	0.16	0.26

our specimens. We anticipate that it could be helpful to point out that even slight changes in the angle of the fracture would result in proppant flowing through the fracture if the proppant was placed while dry. To improve uniformity, we wetted the rock surface with deionized water to prevent this unwanted proppant motion during specimen preparation. To confirm the final loaded proppant mass, we used weight measurements from before and after loading. Minor losses of proppant were recorded during sample handling and were the dominant source of uncertainty ($\pm 5\%$) in the proppant concentrations. The two halves of the specimen were mated together and inserted into a Viton jacket. Special care was taken while inserting the specimen with proppant into the Viton jacket to prevent the movement and loss of proppant. The initial fracture opening was larger when the proppant concentration was 1.0 kg/m² compared with 0.1 kg/m² concentration (Table 1). This is due to proppant arrangement in multiple layers at higher concentration. Two galvanized steel wire tourniquets, one tightened to the core holder and next on the rock specimen, were used on each side of the specimen to ensure the complete isolation of the specimen from the confining fluid and side seal around the rock specimen (Fig. 3c). Finally, the pore pressure lines were connected, and the sample was placed inside the test vessel for testing (Fig. 3d, e).

2.4 Experimental procedure

Our triaxial system was equipped with four pressure intensifiers to apply the radial confining pressure (σ_c), axial normal stress (σ_n), and pore pressures. Prior to applying stress on the specimen, the temperature of the test vessel was increased from room temperature to 130 °C at a nominal rate of 1 °C/min. Once the temperature of the confining fluid inside the test vessel reached 130 °C, the specimen was equilibrated for

12 h. Next, the confining pressure was increased to 15 MPa. The axial stress served as the normal stress (i.e., closure stress) for the propped fracture (Fig. 4).

The test included five stages to impose a stepwise loading–unloading cycle. The closure stress acting on the specimen was increased (i.e., loading) or decreased (i.e., unloading) by 15 MPa in each stage. The closure stress during each step was held constant for 12 h to evaluate the long-term response of the proppant–fracture interaction. The stress was cycled because fracture normal stress in EGS will vary over time and in response to pore fluid pressure changes, such as when injection rates change (Segall 1989; Ellsworth 2013).

To simulate the water flow in an EGS reservoir, deionized water was passed through the fracture in the specimen at 1.33 ml/hr. Thermally equilibrated deionized water was injected into the fracture at its constant temperature of 130 °C. All the experiments in this study were conducted at the same temperature conditions, which allows a direct comparison of proppant pack conductivity. The proppant pack conductivity was measured at the start and end of each stage to investigate the change in conductivity under constant stress condition. The production pressure (i.e., downstream pore pressure) was maintained constant at 5 MPa during all stages of the test. Effluent samples were collected at the end of each stage to measure dissolution and precipitation. Ion concentrations in these samples were measured using Inductively Coupled Plasma—Optical Emission Spectroscopy (ICP-OES). This procedure provides information on the hydro-mechanical-chemical (HMC) response of the proppant pack to better understand and quantify how these processes interacted at our simulated EGS conditions. In addition, Scanning Electron Microscopy (SEM) was used for visual inspection the post-test fractures for evidence of proppant crushing and embedment. Crushed

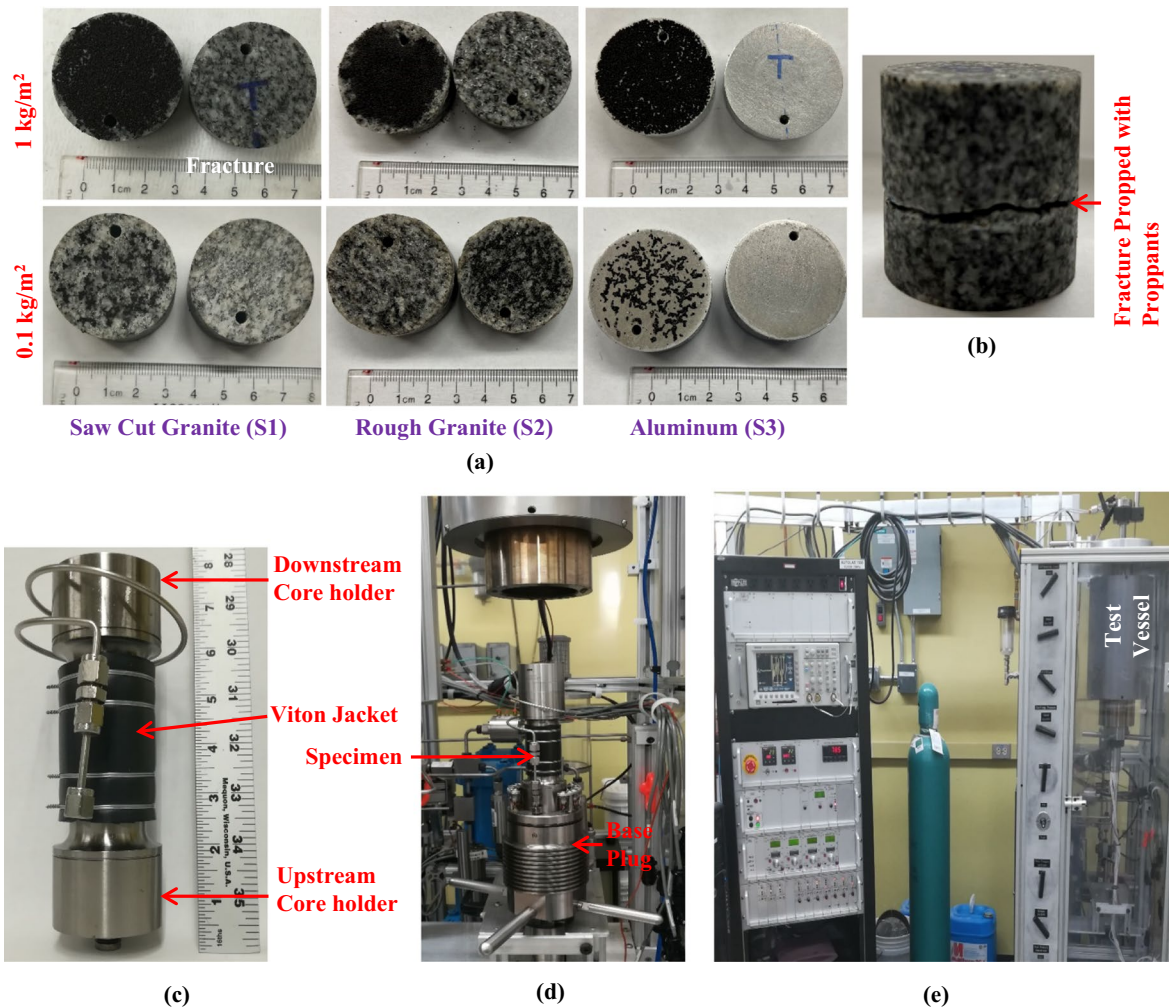


Fig. 3 Test procedure. **a** Proppant placement on the fracture, **b** rough fracture granite specimen with proppant on the fracture, **c** specimen inside the Viton jacket with two core holders

proppant along with any gouge material present on the fracture surface after the completion of experiment was transferred to a metal stub with carbon tape. The particles were then sputter coated with a thin layer of gold–palladium (Au–Pd) to minimize the electric charging effect and increase the quality of the SEM image. To image the fracture surface, the entire surface was sputter coated with a thin layer of Au–Pd and a conductive carbon glue was painted from the fracture surface to the stub to remove the electric charge developed on the fracture surface during imaging.

attached to it, **d** specimen on base plug to be put inside the test vessel, **e** high temperature/temperature triaxial instrument used in the study

2.5 Estimation of fracture conductivity

Barre granite is virtually impermeable due to its low porosity (0.72%). Thus, the dominant flow observed during the experiments was through the fracture. We estimate the conductivity of the fracture using Darcy's law with fixed values for Q and W to ensure cross-comparability of the results as shown below:

$$kw_f = \frac{\mu QL}{W\Delta P} \quad (1)$$

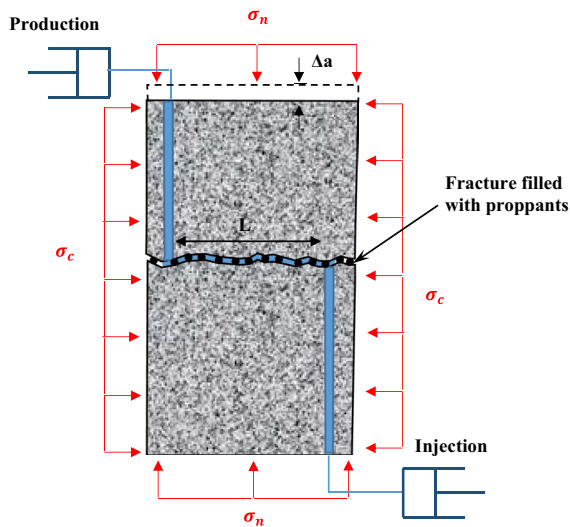


Fig. 4 Schematic showing the stresses and deformation of the specimen during the test

where Q is the steady state flow rate, L is the length of the fracture between two bore holes (28.1 mm), W is the width of the fracture (40.6 mm), ΔP is the differential pore pressure from the injection port to the production port, and μ is the dynamic viscosity of the permeant fluid (deionized water with 2.82×10^{-4} Pa·s at 130 °C). Following the prior work (Ye and Ghassemi 2018), the width of the fracture W was calculated as a width of the rectangular flow region with length L , that has the same area as the fracture. Steady state flow through the fracture was ensured by comparing the injection rate and collection (i.e., production) rate of water. The actual fluid flow is different from the above discussed method. However, this method provides a rapid estimate of conductivity, which serves as a common basis for comparison. For readers who prefer alternative approaches to estimate fracture conductivity, we note that our approach provides the necessary information for conversions that would account for more complex flow, such as for the method proposed by Rutter and Mecklenburgh (2018).

3 Results and discussion

In this section we present our results and discussion organized into five subtopics. All experiments are presented in the order that they relate to: (1) fracture

conductivity, (2) aperture and time, (3) chemical behavior, (4) proppant damage, and (5) implications to field scale EGS.

3.1 Propped fracture conductivity

Figure 5 a–c show the evolution of fracture conductivity with the closure stress at each proppant concentration. The experiments without proppants on the fracture surface i.e., concentration of 0 kg/m² in Fig. 5, was conducted to establish the baseline fracture conductivity at different stress levels. This helps to investigate fracture conductivity enhancement when proppant is placed on the fracture at different concentration under different stress conditions. The conductivity values shown in Fig. 5 are measured at the beginning of the stage, in other words, conductivity right after changing the closure stress. The stress dependency of the propped fracture conductivity can be clearly observed. Use of proppant enhanced the fracture conductivity in all the tests. In particular, conductivity increased by ~4 order of magnitude for saw cut granite (S1), ~5 orders of magnitude for rough granite (S2), and 6 order of magnitude for smooth aluminum (S3) specimen. It is worth noting that the fracture conductivity of saw cut granite was similar to tensile fractured granite, i.e., approximately 2 orders of magnitude higher than for smooth aluminum in the absence of proppant. This could be due to the imperfections in the saw cut fracture surface on the granite specimens. In addition, fracture conductivity of the rough fracture decreases with increase in the closure stress due to closure of the flow paths in rough fracture.

Proppant concentration of 1 kg/m² exhibited higher fracture conductivity than 0.1 kg/m² at all the closure stress levels in granite specimens. Higher proppant concentration results in larger fracture opening (see Table 1) and higher fracture conductivity. As the granite closure stress increased, up to a 50% (0.3 orders of magnitude) decrease in fracture conductivity was observed for both concentrations (Fig. 5). The conductivity of the propped fracture during each stage of all tests are reported in Table 2.

In the case of S3 (i.e., smooth aluminum) with a proppant concentration of 1.0 kg/m², a significant drop in fracture conductivity was observed at the end of the 45 MPa loading stage. A white precipitate, possibly of Aluminum Hydroxide (Al(OH)₃),

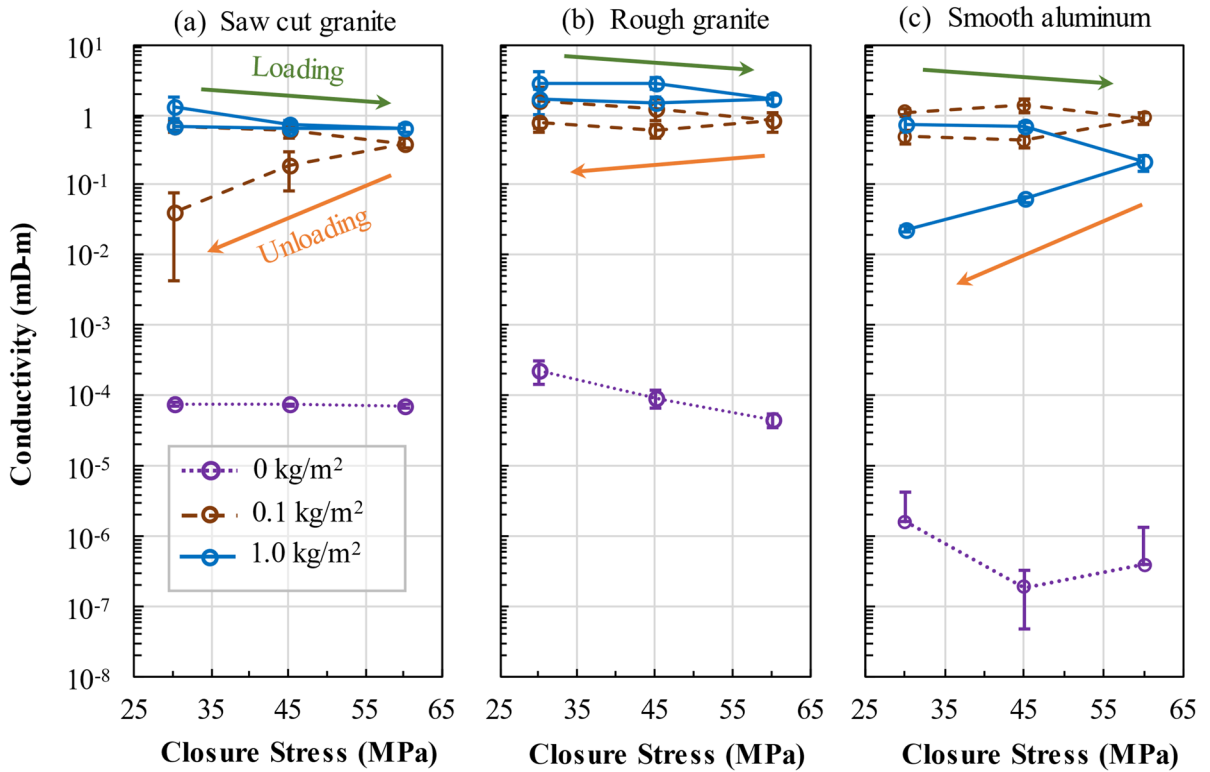


Fig. 5 Conductivity enhancement due to use of proppants on the fracture **a** saw cut granite, **b** rough granite, and **c** smooth aluminum

Table 2 Fracture aperture and permeability values during each stage of the tests

ID	Closure stress (MPa)	Fracture closure (mm)		Conductivity (mD-m)				
		0.1 kg/m ²	1.0 kg/m ²	0 kg/m ²	0.1 kg/m ²		1.0 kg/m ²	
					Start	End	Start	End
S1	30L	0.065	0.079	$7.64 \pm 0.64 \times 10^{-5}$	0.69 ± 0.13	0.57 ± 0.23	1.31 ± 0.45	1.00 ± 0.32
	45L	0.104	0.144	$7.41 \pm 0.38 \times 10^{-5}$	0.59 ± 0.11	0.59 ± 0.09	0.74 ± 0.10	0.78 ± 0.08
	60L	0.150	0.211	$7.27 \pm 0.46 \times 10^{-5}$	0.39 ± 0.06	0.35 ± 0.03	0.64 ± 0.09	0.68 ± 0.07
	45U	0.132	0.176	–	0.19 ± 0.10	0.16 ± 0.15	0.66 ± 0.08	0.64 ± 0.10
	30U	0.098	0.138	–	0.04 ± 0.04	0.05 ± 0.03	0.70 ± 0.09	0.70 ± 0.22
S2	30L	0.076	0.090	$2.30 \pm 0.85 \times 10^{-4}$	1.53 ± 0.96	1.41 ± 0.74	2.89 ± 1.15	2.85 ± 0.67
	45L	0.114	0.151	$9.42 \pm 2.50 \times 10^{-5}$	1.22 ± 0.41	1.04 ± 0.27	2.78 ± 0.52	2.54 ± 1.41
	60L	0.165	0.206	$4.48 \pm 1.01 \times 10^{-5}$	0.81 ± 0.25	0.67 ± 0.19	1.62 ± 0.24	1.64 ± 0.34
	45U	0.145	0.170	–	0.61 ± 0.14	0.67 ± 0.30	1.51 ± 0.26	1.42 ± 0.17
	30U	0.124	0.141	–	0.76 ± 0.13	0.81 ± 0.15	1.69 ± 0.68	1.50 ± 0.25
S3	30L	0.072	0.037	$1.63 \pm 2.54 \times 10^{-6}$	1.10 ± 0.09	1.05 ± 0.13	0.74 ± 0.19	0.72 ± 0.08
	45L	0.095	0.094	$1.86 \pm 1.39 \times 10^{-7}$	1.38 ± 0.30	1.08 ± 0.22	0.68 ± 0.09	0.12 ± 0.04
	60L	0.144	0.133	$3.89 \pm 9.55 \times 10^{-7}$	0.91 ± 0.17	0.46 ± 0.07	0.21 ± 0.05	0.03 ± 0.004
	45U	0.112	0.120	–	0.43 ± 0.08	0.39 ± 0.05	0.06 ± 0.01	0.008 ± 0.001
	30U	0.084	0.105	–	0.48 ± 0.10	0.43 ± 0.06	0.02 ± 0.002	0.01 ± 0.002

L is loading stage and U is unloading stage

was observed at the end of this experiment. The precipitate coated the 200 mesh screens placed at two ends of the specimen, which could be the reason for the unexpected drastic reduction in the permeability observed in this case. Aluminum readily reacts with water to form $\text{Al}(\text{OH})_3$ even at room temperature. However, the reaction does not typically take place because a layer of aluminum oxide naturally coats the aluminum preventing the reaction. In case of smooth aluminum with proppant concentration of 1.0 kg/m^2 , we saw that a few proppants had migrated through the pore fluid hole to the top surface of the aluminum specimen (i.e., not the fracture surface). Since there were very few proppants on this surface, they embedded into the surface and exposed fresh aluminum for reaction.

During the unloading phase of the experiments, all the specimens were unloaded back to initial closure stress levels (i.e., 30 MPa) to examine the effect of proppant concentration on unrecoverable conductivity due to proppant crushing and embedment. However, in recovery of conductivity was negligible in all cases, and the conductivity could even be seen to continue declining in some cases. Total unrecoverable conductivity was higher when the proppant concentration was lower (Fig. 5). At 30 MPa normal stress and the proppant concentration of 0.1 kg/m^2 , 94%, 50%, and 56% of respective initial conductivity remained unrecovered due to proppant crushing and embedment for specimens S1 (saw-cut), S2 (rough), and S3 (aluminum), respectively. The fracture conductivity decrease during the unloading phase was apparently caused by dissolution, precipitation, and migration of fine particles from crushed proppants, as will be further investigated in the next subsections.

Despite the proppant crushing and embedment leading to decline in fracture conductivity, the fracture conductivity was still 4 to 6 orders of magnitude higher when proppant was used to prop the fracture compared to the fracture without proppant. This indicates that while sintered bauxite proppants do risk conductivity loss at in-situ conditions, they retain potential to sustain high conductivity in EGS reservoirs.

3.2 Aperture, conductivity, and time

The fracture aperture reduction due to stress cycling, and its effect on the fracture conductivity

are shown in Figs. 6, 7 and 8. Here we use rock mechanics sign convention (i.e., compression positive) with positive values indicating compression and closure. Mechanical crushing or embedment are prompt, unlike creep, thermal, porous, and chemical processes that take more time (Bandara et al. 2021). Our experiments captured the rapid closure of fracture due to crushing or initial embedment (if it was the dominant aperture reduction modality) and gradual closure due to proppant embedment or creep over time. Fracture closure was observed during the loading phase of all the experiments (Figs. 6, 7 and 8). Subsequent unloading recovered only about 50% of the initial 30 MPa aperture which evidences plastic deformation. In this case, plastic deformation is dominated by proppant crushing and embedment. However, near 100% recovery of the initial aperture was achieved in S3 (aluminum) with a low proppant load of 0.1 kg/m^2 . Also, aperture reduction due to fracture closure in S3 specimen is comparatively lower than the granite samples (S1 and S2) for both proppant concentrations (Table 2). The specifics for why proppant crushing was reduced in this case remains uncertain, but it is reasonable to suspect that this case involved less particle–particle compaction and a more uniform stress field which both help to reduce proppant damage.

In the case of S1 (saw-cut granite) and S2 (rough granite) specimens, the fracture aperture reduction due to fracture closure was 20% to 30% higher when the proppant concentration was 1.0 kg/m^2 compared to that of 0.1 kg/m^2 (Table 2). In the case of a 0.1 kg/m^2 concentration, the proppant was laid down as a sparse monolayer, whereas the proppants are arranged in multiple layers when the concentration was 1.0 kg/m^2 (Fig. 3). As will soon be shown using scanning electron microscopy (SEM), the deformation of the higher proppant loading seems to have been dominated by particle packing and rearrangement while the deformation at lower proppant loading was dominated by proppant crushing. This study did not seek to identify an optimal proppant loading because proppant distribution in fractures in the field is notoriously difficult to control and is unlikely to be optimally placed.

Fracture conductivity was measured with nominally three or more datapoints at the beginning and end of each stage to examine its evolution under a constant stress and temperature. Fracture conductivity

Fig. 6 Evolution of fracture closure and conductivity in S1 (saw cut granite) specimen for proppant concentration of **a** 0.1 kg/m², and **b** 1.0 kg/m²

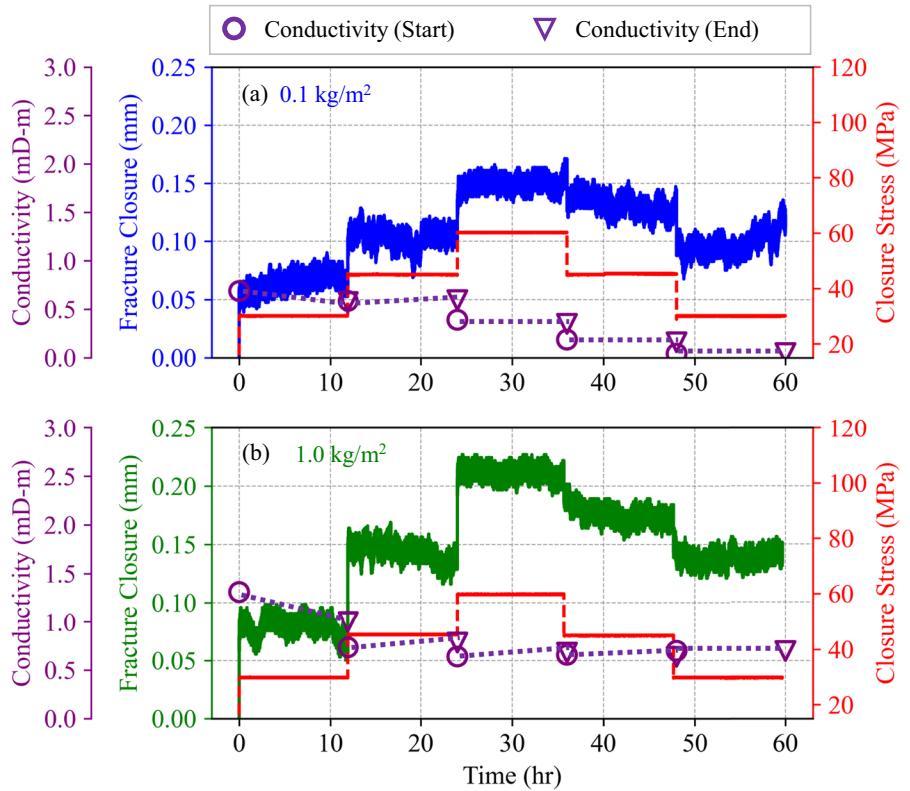


Fig. 7 Evolution of fracture closure and conductivity in S2 (tensile induced rough fractured granite) specimen for proppant concentration of **a** 0.1 kg/m², and **b** 1.0 kg/m²

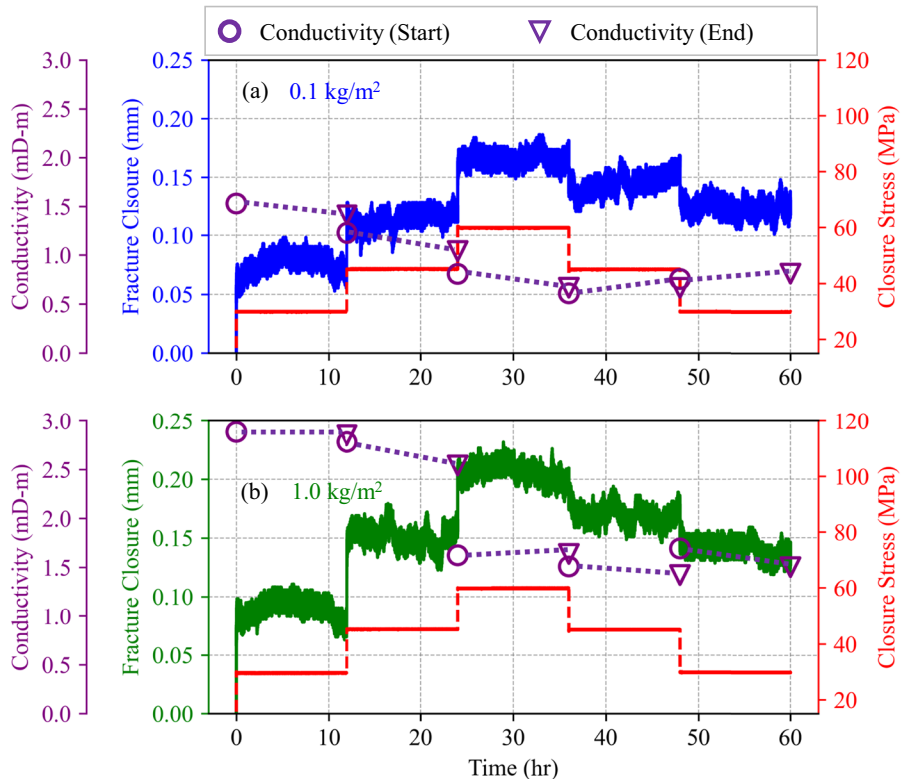
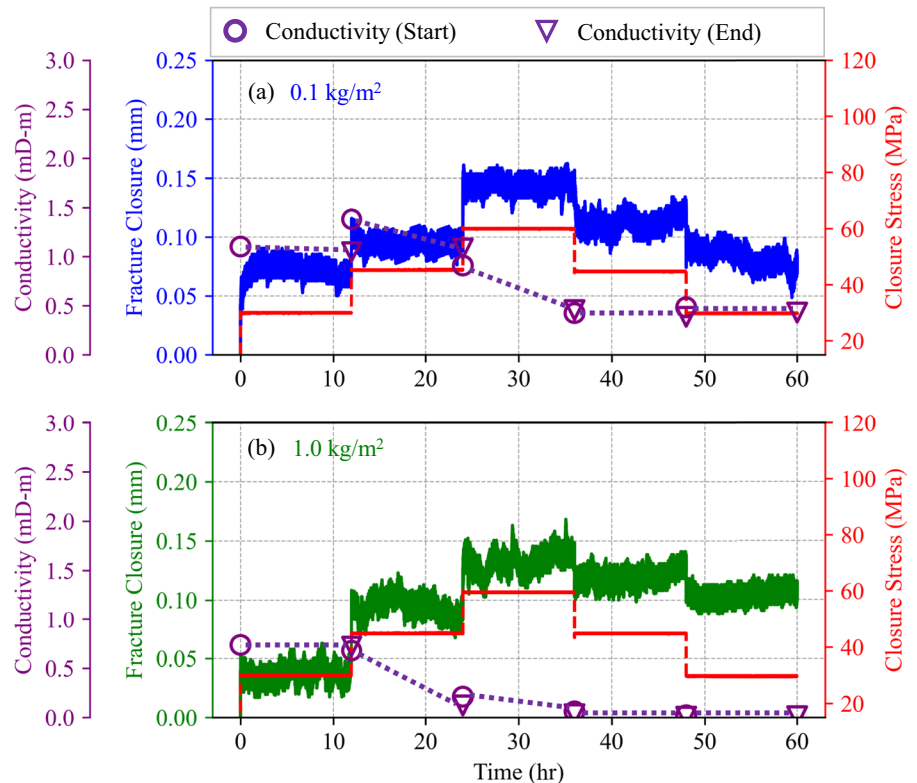


Fig. 8 Evolution of fracture closure and conductivity in S3 (smooth aluminum) specimen for a proppant concentration of **a** 0.1 kg/m², and **b** 1.0 kg/m²



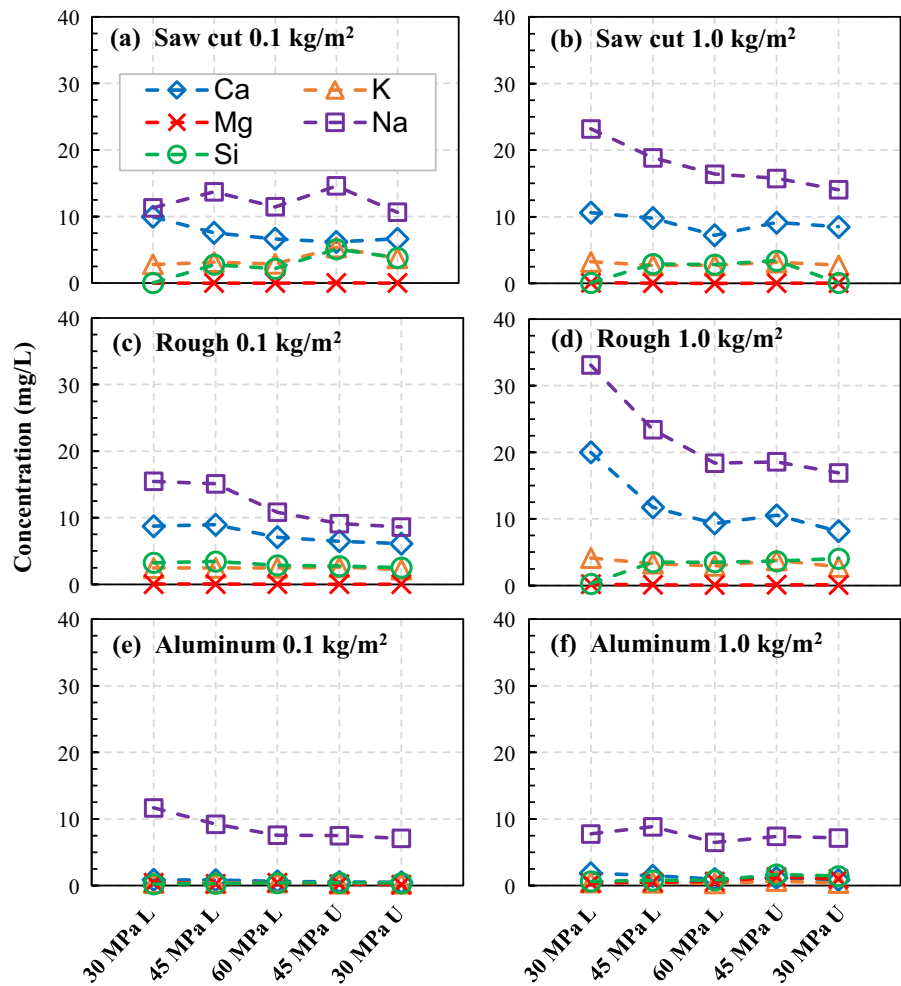
at the beginning of the stage is represented by purple circles and that at the end of the stage is represented by purple triangles in Figs. 6, 7 and 8. For clarity, conductivities at the start and end of the same stage are connected by a dashed purple line. These conductivity values are also reported in Table 2. Conductivity of the propped fractures promptly decreased with increasing closure stress during the loading stages in conjunction with the aperture reduction. In contrast, fracture conductivity at the end of the stage decreased or remained consistent with that of the beginning of the stage while having the overall trend of decreasing conductivity over time. This result is consistent with the prompt conductivity loss due to proppant crushing, embedment, and packing when the closure stress is increased during each stage. The crushed proppant and fines migrate under constant state of stress to clog the flow path and decrease the conductivity at the end of the stage as observed during some stages in this study. The conductivity loss due to creep, thermal, and chemical effects were expected to be negligible because 60 h of test duration is relatively brief with respect to these slower phenomena. However, it should be noted that these effects will continue to

impact the fracture conductivity in the timescale of the reservoir operation.

3.3 Chemical behavior

The results of ICP-OES analysis on the effluent solutions collected at the end of each stage are shown in Fig. 9. Al, Ca, Fe, K, Mg, Na, and Si in the effluent sample indicate dissolution of minerals from the rock and proppant during the tests, with higher concentrations indicating faster dissolution because flow rates and residence times were constant. In this study, tests on the aluminum specimen were intended to investigate the dissolution of constituents solely from the proppant, but we suspect that embedment may have caused the aluminum substrate to be reactive as well. The concentration of Ca, K, Na, and Si in the effluent indicates the dissolution of feldspar and quartz minerals present in the Barre granite (Caulk et al. 2016; Bijay and Ghazanfari 2021). Moreover, sintered bauxite proppant could also serve as a source for these elements. According to the manufacturer, the proppant is composed of 83.0% Al₂O₃, 5.0% SiO₂, 7.0% Fe₂O₃, 3.5% TiO₂ and 1.5% of minor components such as

Fig. 9 Dissolution of minerals at the end of each stage during the tests for **a** and **b** saw cut granite, **c** and **d** rough granite, **e** and **f** aluminum specimen. The left column i.e. **a**, **c** and **e** are for proppant concentration of 0.1 kg/m² and the right column i.e. **b**, **d**, and **f** are for proppant concentration of 1.0 kg/m²



K₂O, CaO, MgO, Na₂O, MnO, and others (Siegel et al., 2015). Very small concentrations of Mg and non-detectable Fe concentration in the effluent solution indicates the dissolution of biotite and chlorite from Barre granite was insignificant. Al, which is the major constituent in bauxite (proppant) and feldspar in granite, was not detected in any sample. The non-detectable Al and high concentration of Ca, Na, and K in the effluent indicates the possibility of formation of kaolinite, which precipitates in the system (Caulk et al. 2016).

Concentrations of all the detected ions (Ca, K, Mg, Na, and Si) were higher at proppant concentration of 1.0 kg/m² compared to 0.1 kg/m² in all the tests. In addition, the concentrations were highest during the first stage (i.e., 30 MPa loading). This indicates that crushing and embedment of proppants into the fracture surface exposes new surface, which

increase the dissolution of minerals in the system. The concentration of Na and Ca is higher than other elements because salt rich in Ca and Na are more readily dissolvable than silicates. Moreover, the reaction involving the formation of Kaolinite from feldspar (oligoclase and microcline) releases Ca, K, and Na ions (Caulk et al. 2016), which could also have contributed to the elevated concentration of these elements in the solution. As seen in Fig. 9, the concentrations of Ca, K, Na, and Si in the effluents from the aluminum specimen (S3) are smaller compared to granite specimens (S1 and S2) under similar conditions. This indicates the dissolution rate of minerals is higher from rock-proppant system compared to that from the proppant alone. Nevertheless, ions in the effluents from S3 specimen indicates that sintered bauxite proppants will dissolve under the high

temperatures and pressures encountered in EGS, which will negatively impact long-term performance.

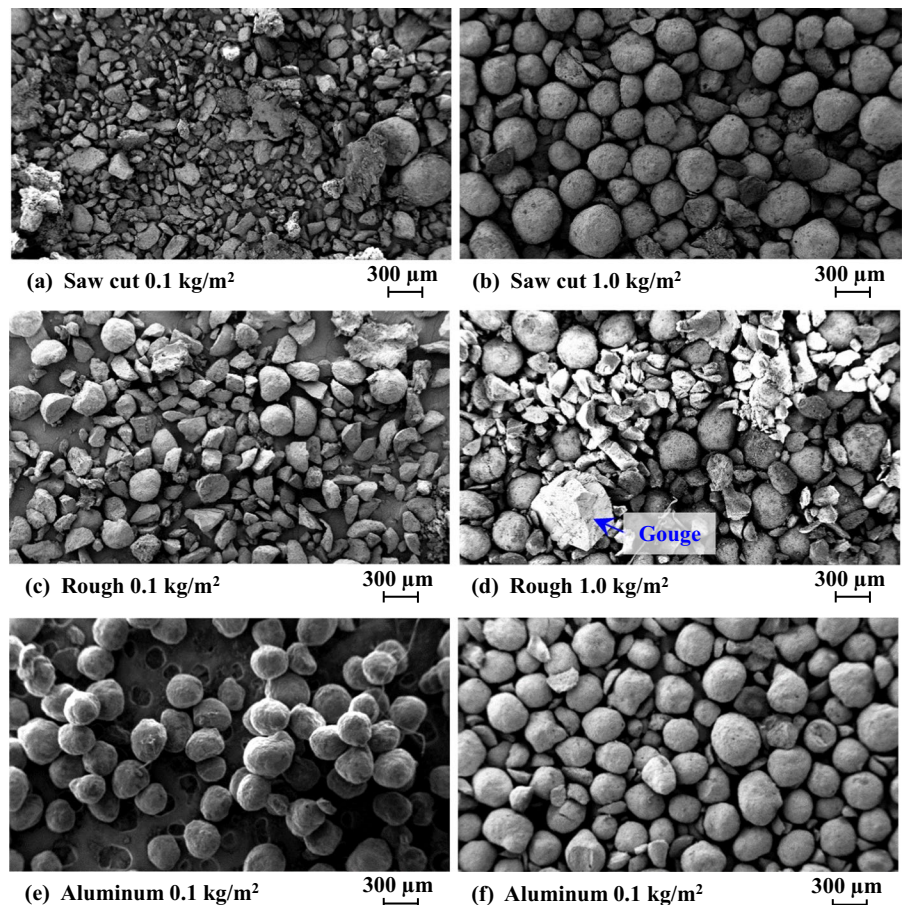
3.4 Visual analysis of proppant damage

Scanning Electron Microscopy (SEM) imaging was carried out on the post-test proppants and the fracture surfaces to assess crushing and embedment as well as possible precipitation of secondary minerals (Fig. 10). In the granite specimens, pervasive proppant crushing was observed at the 0.1 kg/m² concentration. In contrast, intact proppant particles were more common at 1.0 kg/m². At the lower concentration with its sparse monolayer, the stress acting on individual proppant particles will be higher which should result in more crushing unless the particles embed into the host rock (Tang et al. 2018; Bandara et al. 2019). Moreover, the proppant crushed into finer particles in the case of S1 specimen at 0.1 kg/m² concentration compared to the S2 specimen at same concentration. This indicates

that a smooth fracture surface can promote more particle crushing than rougher surfaces. Large gouge particles (up to ~1 mm in size) from asperities from the fracture surface were also observed in S2 (rough granite) specimen, suggesting more fracture surface damage or softer surfaces in the rough fracture. Fines produced as a result of proppant crushing and asperity damage move in the flow direction, blocking pore throats and leading to permeability decline over time (Fan and Chen 2020). Moreover, these fines could also enhance the dissolution/precipitation in the proppant-fracture system leading to permeability decline in long-run (Caulk et al. 2016; Vogler et al. 2016; Bijay and Ghazanfari 2021).

Indentation on the fracture surface left by proppants after the test was observed in the saw-cut granite and aluminum. The indentation was difficult to visualize on the rough granite surface. However, the SEM images show that the proppant embedded into the fracture surface and remain attached on the

Fig. 10 Proppant crushing is higher at lower proppant concentration. **a, b** saw cut granite (S1) specimen, **c, d** rough granite (S2) specimen, and **e, f** smooth aluminum (S3) specimen. The left column i.e. **a, c** and **e** are for proppant concentration of 0.1 kg/m² and the right column i.e. **b, d**, and **f** are for proppant concentration of 1.0 kg/m²



rough granite (S2) surface (Fig. 11). In the case of the saw cut specimen (S1), the proppant left indentation marks due to embedment, however the proppants did not attach on the smooth surface of the fracture. In addition, a secondary cracking from the embedment locations were observed in saw cut granite. These secondary cracks weaken the fracture surface resulting in spalling of particles from the surface and clogging the flow path.

3.5 Implication for EGS

Proppants have potential to sustain the conductivity of fractures in EGS reservoirs. Also, proppants eliminate the necessity of other stimulation techniques such as shear stimulation or hydraulic propping (Norbeck et al. 2018; Frash et al. 2023a, b) for permanent permeability enhancement. Use of proppants can help to reduce injection pressures to mitigate the risk of induced seismicity in EGS, which is otherwise a hurdle for EGS development (Majer et al. 2007; Deichmann and Giardini 2009). In addition, with the development of stimulation techniques such as thermal and electrical stimulation (Tarasovs and Ghassemi 2011; Breede et al. 2013; Bauer et al. 2015), which induce tensile fractures similarly to hydraulic fracturing, proppants retain a huge potential to be used in future EGS applications. The results from this experiment indicate that proppant, even at very low concentration, can enhance the fracture conductivity by orders of magnitude. However, these proppants will crush, embed, and dissolve at in-situ conditions to create fines and reactive surface area that will reduce the conductivity in long-run (Vogler et al. 2016; Ye and Ghassemi 2018; Bandara et al. 2021). It is worth noting that conductivity loss in a fracture due to proppant crushing, embedment, fines migration, mineral dissolution, and precipitation under

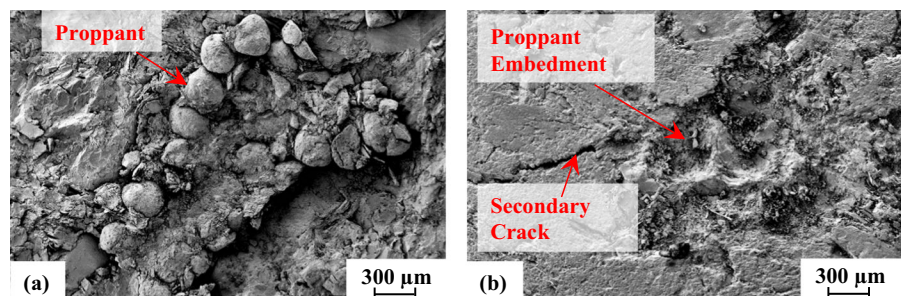
EGS conditions is a complex coupled problem. Our results show that proppant can sustain fracture conductivity after crushing and embedment under stress in the short-term (< 60 h). However, conductivity loss due to creep, chemical processes and fines migration in the proppant pack will act at longer timescales than the test duration in this study, so we were unable to quantify this effect even though we suspect that these processes could be important for long term EGS productivity.

As expected, the effluent chemistry indicated dissolution of minerals from the rock as well as proppants under EGS condition. Dissolved minerals will lead to precipitation of secondary minerals (Brinton et al. 2011; Jones et al. 2014) and scaling problems in wells, pipes, and accessories used in the plants (Xu et al. 2004; André et al. 2006). In addition, leaching of minerals from the proppants could reduce the strength leading to reduced crush resistance over time (Mattson et al. 2016). This will result in performance losses for EGS over time.

4 Conclusions

Laboratory flow-through experiments were conducted on saw-cut granite, rough fractured granite, and aluminum specimens filled with three different concentrations of sintered bauxite proppant. All fractured samples were subjected to low-enthalpy EGS conditions of 130 °C and up to 60 MPa normal stress, suitable for Organic Rankine or Binary electrical power production. Proppant successfully maintained the fracture conductivity at levels from 4 to 6 orders of magnitude higher than without, peaking at a conductivity of 3 mD-m. However, direct evidence of proppant dissolution, crushing, and embedment was also observed in all experiments using stress-cycle plastic

Fig. 11 Proppant embeds and remain attached into the **a** rough fracture surface. **b** secondary cracks could propagate from embedment location as seen in saw cut granite



deformation measurements, hydraulic conductivity measurements over a 60 h period, post-test fracture surface SEM, and effluent ICP-OES. Ultimately, these results indicate that sintered bauxite holds promise for increasing fracture conductivity in the field while also confirming that the benefit of proppant will significantly diminish over time.

Acknowledgements This research was funded by Department of Energy (DOE) Basic Energy Sciences under FWP LANLE3W1. Support was also provided by the Los Alamos National Laboratory's Laboratory Directed Research and Development—Directed Research program (LDRD-20230022DR). Rock of Ages quarry in Barre, Vermont donated granite samples. Carbo Ceramics donated CARBOBEAD HSP proppants. We would also like to thank editors and reviewers for their valuable comments and suggestions.

Author contributions BK: Conceptualization, Methodology, Investigation, Visualization, Writing-Original Draft. EG: Conceptualization, Supervision, Writing-Review and Editing. JM: Conceptualization, Supervision, Writing-Review and Editing. LF: Funding acquisition, Writing-Review and Editing. MM: Writing-Review and Editing. All authors read and approved the final manuscript.

Funding This research was funded by Department of Energy (DOE) Basic Energy Sciences under FWP LANLE3W1 for supporting this work. Support was also provided by the Los Alamos National Laboratory's Laboratory Directed Research and Development—Directed Research program (LDRD-20230022DR).

Data availability All the data and codes generated in this study of this study are available from the corresponding author upon reasonable request.

Declarations

Ethics approval and consent to participate This manuscript has not been published and is not under consideration for publication elsewhere.

Consent for publication The authors declare that they have all agreed to publish the work reported in this paper.

Competing interests The authors have no relevant financial or non-financial interests to disclose.

Open Access This article is licensed under a Creative Commons Attribution 4.0 International License, which permits use, sharing, adaptation, distribution and reproduction in any medium or format, as long as you give appropriate credit to the original author(s) and the source, provide a link to the Creative Commons licence, and indicate if changes were made. The images or other third party material in this article are included

in the article's Creative Commons licence, unless indicated otherwise in a credit line to the material. If material is not included in the article's Creative Commons licence and your intended use is not permitted by statutory regulation or exceeds the permitted use, you will need to obtain permission directly from the copyright holder. To view a copy of this licence, visit <http://creativecommons.org/licenses/by/4.0/>.

References

- André L, Rabemanana V, Vuataz FD (2006) Influence of water-rock interactions on fracture permeability of the deep reservoir at Soultz-sous-Forêts, France. *Geothermics* 35(5–6):507–531. <https://doi.org/10.1016/j.geothermics.2006.09.006>
- Augustine C, Ho J, Blair N (2019) GeoVision analysis supporting task force report: electric sector potential to penetration. NREL (No. NREL/TP-6A20-71833)
- Bagepalli MV, Yarrington JD, Schrader AJ, Zhang ZM, Ranjan D, Loutzenhiser PG (2020) Measurement of flow properties coupled to experimental and numerical analyses of dense, granular flows for solar thermal energy storage. *Sol Energy* 207:77–90. <https://doi.org/10.1016/j.solener.2020.06.062>
- Bandara KMAS, Ranjith PG, Rathnaweera TD (2019) Proppant crushing mechanisms under reservoir conditions: insights into long-term integrity of unconventional energy production. *Nat Resour Res* 28(3):1139–1161. <https://doi.org/10.1007/s11053-018-9441-0>
- Bandara KMAS, Ranjith PG, Haque A, Wanniarachchi WAM, Zheng W, Rathnaweera TD (2021) An experimental investigation of the effect of long-term, time-dependent proppant embedment on fracture permeability and fracture aperture reduction. *Int J Rock Mech Min Sci* 144:104813. <https://doi.org/10.1016/j.ijrmms.2021.104813>
- Barboza BR, Chen B, Li C (2021) A review on proppant transport modelling. *J Pet Sci Eng* 204:1–27. <https://doi.org/10.1016/j.petrol.2021.108753>
- Bauer S, Geilikman M, Gardner P, Broome S, Glover S, Williamson K, Su J (2015) Water-free shale stimulation: experimental studies of electrofracturing. AGU Fall Meet. Abstr. (MR41C-2644)
- Benson ME, Wilson AB (2015) Frac sand in the united states—a geological and industrial overview. USGS, 2015-1107. <https://doi.org/10.3133/ofr20151107>
- Bijay KC, Ghazanfari E (2021) Geothermal reservoir stimulation through hydro-shearing: an experimental study under conditions close to enhanced geothermal systems. *Geothermics* 96:102200. <https://doi.org/10.1016/j.geothermics.2021.102200>
- Bradford J, McLennan J, Moore J, Glasby D, Waters D, Kruwell R, Bailey A, Rickard W, Bloomfield K, King D (2013) Recent developments at the Raft River geothermal field. 38th Workshop on Geothermal Reservoir Engineering, Stanford University

- Breede K, Dzebisashvili K, Liu X, Falcone G (2013) A systematic review of enhanced (or engineered) geothermal systems: past, present and future. *Geotherm Energy* 1(1):1–27. <https://doi.org/10.1186/2195-9706-1-4>
- Brinton D, McLin K, Moore J (2011) The chemical stability of bauxite and quartz sand proppant under geothermal conditions. 36th Workshop on Geothermal Reservoir Engineering, Stanford University
- Caulk RA, Ghazanfari E, Perdril JN, Perdril N (2016) Experimental investigation of fracture aperture and permeability change within enhanced geothermal systems. *Geothermics* 62:12–21. <https://doi.org/10.1016/j.geothermics.2016.02.003>
- Chun T, Li Y, Wu K (2020) Comprehensive experimental study of proppant transport in an inclined fracture. *J Pet Sci Eng* 184:106523. <https://doi.org/10.1016/j.petrol.2019.106523>
- Cladouhos TT, Petty S, Swyer MW, Uddenberg ME, Grasso K, Nordin Y (2016) Results from Newberry Volcano EGS Demonstration, 2010–2014. *Geothermics* 63:44–61. <https://doi.org/10.1016/j.geothermics.2015.08.009>
- Deichmann N, Giardini D (2009) Earthquakes induced by the stimulation of an enhanced geothermal system below Basel (Switzerland). *Seismol Res Lett* 80(5):784–798. <https://doi.org/10.1785/gssrl.80.5.784>
- EIA (2022) Geothermal explained: use of geothermal energy. <https://www.eia.gov/energyexplained/geothermal/use-of-geothermal-energy.php>. Accessed 11 Aug 2022
- Ellsworth WL (2013) Injection-induced earthquakes. *Science* 341(6142):1–8. <https://doi.org/10.1126/science.1225942>
- Fan M, Chen C (2020) Numerical simulation of the migration and deposition of fine particles in a proppant-supported fracture. *J Pet Sci Eng* 194:107484. <https://doi.org/10.1016/j.petrol.2020.107484>
- Frash LP, Sweeney M, Meng M, Bijay KC, Iyare UC, Madenova Y, Carey JW, Li W (2023a) Exploring the limitations of fracture caging in nextgen enhanced geothermal systems. In: Proceedings of the 57th US rock mechanics/geomechanics symposium, Atlanta, GA, USA, 25–28 June. <https://doi.org/10.56952/ARMA-2023-0052>
- Frash LP, Carey JW, Ahmmed B, Sweeney M, Meng M, Li W, Bijay KC, Iyare U (2023b) A proposal for safe and profitable enhanced geothermal systems in hot dry rock. 48th Workshop on Geothermal Reservoir Engineering, Stanford University
- Fredd CN, McConnell SB, Boney CL, England KW (2000) Experimental study of hydraulic fracture conductivity demonstrates the benefits of using proppants. SPE Rocky Mt. Reg. Meet. Proc. <https://doi.org/10.2523/60326-ms>
- Ghassemi A (2012) A review of some rock mechanics issues in geothermal reservoir development. *Geotech Geol Eng* 30(3):647–664. <https://doi.org/10.1007/s10706-012-9508-3>
- Häring MO, Schanz U, Ladner F, Dyer BC (2008) Characterisation of the Basel 1 enhanced geothermal system. *Geothermics* 37(5):469–495. <https://doi.org/10.1016/j.geothermics.2008.06.002>
- Huenges E, Holl HG, Legarth B, Zimmermann G, Saadat A (2004) The stimulation of a sedimentary geothermal reservoir in the North German basin: case study Groß Schönebeck. 29th Workshop on Geothermal Reservoir Engineering, Stanford University
- Jones CG, Simmons SF, Moore JN (2014) Proppant behavior under simulated geothermal reservoir conditions. 39th Workshop on Geothermal Reservoir Engineering, Stanford University
- Liang F, Sayed M, Al-Muntasheri GA, Chang FF, Li L (2016) A comprehensive review on proppant technologies. *Petroleum* 2(1):26–39. <https://doi.org/10.1016/j.petlm.2015.11.001>
- Majer EL, Baria R, Stark M, Oates S, Bommer J, Smith B, Asanuma H (2007) Induced seismicity associated with Enhanced Geothermal Systems. *Geothermics* 36(3):185–222. <https://doi.org/10.1016/j.geothermics.2007.03.003>
- Mattson ED, Neupane G, Plummer M, Jones C, Moore J (2016) Long-term sustainability of fracture conductivity in geothermal systems using proppants. 41st Workshop Geothermal Reservoir Engineering, Stanford University
- McLin K, Brinton D, Mandalaparty P, Jones C, Moore J (2010) The chemical and thermal stability of proppants under geothermal conditions. *Geotherm Resour Coun Trans* 34:397–402
- Meng M, Frash LP, Li W, Welch NJ, Carey JW, Morris J, Neupane G, Ulrich C, Kneafsey T (2022) Hydro-mechanical measurements of sheared crystalline rock fractures with applications for EGS Collab Experiments 1 and 2. *J Geophys Res Solid Earth* 127(2):1–22. <https://doi.org/10.1029/2021JB023000>
- Norbeck JH, McClure MW, Horne RN (2018) Field observations at the Fenton Hill enhanced geothermal system test site support mixed-mechanism stimulation. *Geothermics* 74:135–149. <https://doi.org/10.1016/j.geothermics.2018.03.003>
- Norbeck J, Latimer T, Gradl C, Agarwal S, Dadi S, Eddy E, Fercho S, Lang C, McConville E, Titov A, Voller K, Woitt M (2023) A review of drilling, completion, and stimulation of a horizontal geothermal well system in North-Central Nevada. 48th Workshop on Geothermal Reservoir Engineering, Stanford University
- Penny GS (1987) An evaluation of the effects of environmental conditions and fracturing fluids upon the long-term conductivity of proppants. In: SPE annual technical conference and exhibition, Dallas, TX. SPE
- Portier S, Vuataz FD, Nami P, Sanjuan B, Gérard A (2009) Chemical stimulation techniques for geothermal wells: experiments on the three-well EGS system at Soultz-sous-Forêts, France. *Geothermics* 38(4):349–359. <https://doi.org/10.1016/j.geothermics.2009.07.001>
- Rutqvist J, Jeanne P, Dobson PF, Garcia J, Hartline C, Hutchings L, Singh A, Vasco DW, Walters M (2016) The Northwest Geysers EGS Demonstration Project, California—Part 2: modeling and interpretation. *Geothermics* 63:120–138. <https://doi.org/10.1016/j.geothermics.2015.08.002>
- Rutter EH, Mecklenburgh J (2018) Influence of normal and shear stress on the hydraulic transmissivity of thin cracks in a tight quartz sandstone, a granite, and a shale. *J Geophys Res Solid Earth* 123(2):1262–1285. <https://doi.org/10.1002/2017JB014858>
- Sahai R, Moghanloo RG (2019) Proppant transport in complex fracture networks—a review. *J Pet Sci Eng* 182:106199. <https://doi.org/10.1016/j.petrol.2019.106199>

- Schill E, Genter A, Cuenot N, Kohl T (2017) Hydraulic performance history at the Soultz EGS reservoirs from stimulation and long-term circulation tests. *Geothermics* 70:110–124. <https://doi.org/10.1016/j.geothermics.2017.06.003>
- Segall P (1989) Earthquakes triggered by fluid extraction. *Geology* 17(10):942–946. [https://doi.org/10.1130/0091-7613\(1989\)017%3c0942:ETBFE%3e2.3.CO;2](https://doi.org/10.1130/0091-7613(1989)017%3c0942:ETBFE%3e2.3.CO;2)
- Shiozawa S, McClure M, Keeton ED (2014) EGS designs with horizontal wells, multiple stages, and proppant. 39th Work Geothermal Reservoir Engineering, Stanford University
- Tang Y, Ranjith PG, Perera MS, Rathnaweera TD (2018) Influences of proppant concentration and fracturing fluids on proppant-embedment behavior for inhomogeneous rock medium: an experimental and numerical study. *SPE Prod Oper* 33(04):666–678. <https://doi.org/10.2118/189984-PA>
- Tarasovs S, Ghassemi A (2011) Propagation of a system of cracks under thermal stress. In: Proceedings of the 45th U.S. Rock Mechanics/Geomechanics Symposium, San Francisco, CA, 26–29 June
- Tester JW, Anderson BJ, Batchelor AS, Blackwell DD, DiPippo R (2006) The future of geothermal energy—impact of Enhanced Geothermal Systems (EGS) on the United States in the 21st century. MIT—Massachusetts Institute of Technology, p 358
- Tomac I, Sauter M (2018) A review on challenges in the assessment of geomechanical rock performance for deep geothermal reservoir development. *Renew Sustain Energy Rev* 82:3972–3980. <https://doi.org/10.1016/j.rser.2017.10.076>
- Vogler D, Amann F, Bayer P, Elsworth D (2016) Permeability evolution in natural fractures subject to cyclic loading and gouge formation. *Rock Mech Rock Eng* 49(9):3463–3479. <https://doi.org/10.1007/s00603-016-1022-0>
- Williams CF, Reed MJ, Mariner RH, DeAngelo J, Galanis SPJ (2008) sAssessment of moderate-and high-temperature geothermal resources of the United States. U.S. Geol. Surv. Fact Sheet 2008-3082, pp 1–4
- Xu T, Ontoy Y, Molling P, Spycher N, Parini M, Pruess K (2004) Reactive transport modeling of injection well scaling and acidizing at Tiwi field, Philippines. *Geothermics* 33(4):477–491. <https://doi.org/10.1016/j.geothermics.2003.09.012>
- Ye Z, Ghassemi A (2018) Injection-induced shear slip and permeability enhancement in granite fractures. *J Geophys Res Solid Earth* 123(10):9009–9032. <https://doi.org/10.1029/2018JB016045>
- Zhang Y, Wu Y, Teng Y, Li P, Peng S (2022) Experiment study on the evolution of permeability and heat recovery efficiency in fractured granite with proppants. *Geomech Geophys Geo-Energy Geo-Resour* 8(1):3. <https://doi.org/10.1007/s40948-021-00306-w>
- Zimmermann G, Reinicke A (2010) Hydraulic stimulation of a deep sandstone reservoir to develop an Enhanced Geothermal System: laboratory and field experiments. *Geothermics* 39(1):70–77. <https://doi.org/10.1016/j.geothermics.2009.12.003>

Publisher's Note Springer Nature remains neutral with regard to jurisdictional claims in published maps and institutional affiliations.